A&A 448, 861–871 (2006)
DOI: 10.1051/0004-6361:20053644

Astronomy & Astrophysics

Log-parabolic spectra and particle acceleration in blazars

III. SSC emission in the TeV band from Mkn 501

E. Massaro[1], A. Tramacere[1], M. Perri[2], P. Giommi[2], and G. Tosti[3]

[1] Dipartimento di Fisica, Università La Sapienza, Piazzale A. Moro 2, 00185 Roma, Italy
e-mail: enrico.massaro@uniroma1.it
[2] ASI Science Data Center, ESRIN, 00044 Frascati, Italy
[3] Dipartimento di Fisica, Università di Perugia, via A. Pascoli, Perugia, Italy

Received 16 June 2005 / Accepted 11 October 2005

ABSTRACT

Curved broad-band spectral distributions of non-thermal sources like blazars are described well by a log-parabolic law where the second degree term measures the curvature. Log-parabolic energy spectra can be obtained for relativistic electrons by means of a statistical acceleration mechanism whose probability of acceleration depends on energy. In this paper we compute the spectra radiated by an electron population via synchrotron and Synchro-Self Compton processes to derive the relations between the log-parabolic parameters.
These spectra were obtained by means of an accurate numerical code that takes the proper spectral distributions for single particle emission into account.
We found that the ratio between the curvature parameters of the synchrotron spectrum to that of the electrons is equal to ∼0.2 instead of 0.25, the value foreseen in the δ-approximation. Inverse Compton spectra are also intrinsically curved and can be approximated by a log-parabola only in limited ranges. The curvature parameter, estimated around the SED peak, may vary from a lower value than that of the synchrotron spectrum up to that of emitting electrons depending on whether the scattering is in the Thomson or in the Klein-Nishina regime. We applied this analysis to computing the synchro-self Compton emission from the BL Lac object Mkn 501 during the large flare of April 1997. We fit simultaneous *Beppo*SAX and CAT data and reproduced intensities and spectral curvatures of both components with good accuracy.
The large curvature observed in the TeV range was found to be mainly intrinsic, and therefore did not require a large pair production absorption against the extragalactic background. We regard this finding as an indication that the Universe is more transparent at these energies than previously assumed by several models found in the literature. This conclusion is supported by recent detection of two relatively high redshift blazars with HESS.

Key words. radiation mechanisms: non-thermal – galaxies: active – BL Lacertae objects: general – BL Lacertae objects: individual: Mkn 501

1. Introduction

The spectral energy distributions (SEDs) of blazars, and particularly of BL Lac objects, are characterised by a double-peak structure. The peak at lower energies is generally explained by synchrotron radiation from relativistic electrons in a jet that is closely aligned to the line of sight, while the high frequency bump is produced by inverse Compton scattering from the same electron population interacting either with the synchrotron photons (SSC, Synchrotron-Self Compton models, see e.g. Marscher & Gear 1985) or with other photons that originated in the local environment (ERC, External Radiation Compton models, see e.g. Sikora et al. 1994).

For the so-called Low-energy peaked BL Lac (LBL) objects, the frequency of the first peak is in the Infrared-Optical region, while it is in the UV−X ray range for the High-energy peaked BL Lac (HBL) (Padovani & Giommi 1995). The shape of these bumps is characterised in the Log(νF_ν) vs. Log ν plot by a rather smooth curvature extending through several frequency decades. A very simple and successful analytical function that can model the shape of these broad peaks is a parabola in the logarithms of the variables (hereafter log-parabola). This function has only three spectral parameters, and was used by Landau et al. (1986) to fit the broad band spectra of some bright BL Lac objects from radio to UV. Sambruna et al. (1996) also used a log-parabola to fit blazars' SED to estimate peak frequencies and luminosities without, however, attributing a physical meaning to this shape. In two previous papers (Massaro et al. 2004a,b, hereafter Paper I and Paper II, respectively) we used the log-parabolic model to fit the BeppoSAX broad band X-ray spectra of the BL Lac objects Mkn 421 and Mkn 501 and studied the relations between the spectral parameters and the luminosity. We also showed that, under simple approximations, a log-parabolic synchrotron spectrum can be obtained by

a relativistic electron population having a similar energy distribution, and then derived the main relations between their parameters. Furthermore, in Paper I we proposed a simple explanation for the log-parabolic energy distribution of the electrons as resulting from a statistical mechanism where the acceleration probability decreases with the particle energy.

Curved spectra in non-thermal sources have already been studied in the past and generally were related to the radiative ageing of the emitting electrons that have a single power law injection spectrum. The well-known solution by Kardashev (1962) predicts a change in the electron spectral index by a unity (0.5 for the synchrotron spectrum) around a break energy, whose value decreases with time. Probably for this reason, curved spectra have been modelled by means of rather complex functions like a double broken power law (Kataoka et al. 1999) or a continuous combination of two power laws after releasing the condition on the difference of spectral indices (see the discussion in Fossati et al. 2000). A similar spectrum is generally used in the spectral modelling of gamma-ray bursts (Band et al. 1993). On the same basis, Sohn et al. (2003) more recently introduced a spectral-curvature parameter, defined as the difference between two spectral indices in different frequency intervals, to study the evolution of synchrotron sources. As we will show later, this parameter is strongly dependent on the chosen frequency range and cannot be univocally related to the actual curved shapes.

In this paper we stress the advantages of using a log-parabolic law to model curved spectra over broad frequency ranges and present the results of an accurate study of the spectral distributions of the synchrotron radiation (hereafter SR) and of the inverse Compton (hereafter IC) scattered photons by a population of relativistic electrons with such energy spectrum. We study, in particular, the relations between the parameters of SR spectra and those of the electrons and show that they are generally approximated well by simple power behaviours and that they provide useful information on the electron spectrum. The relations with the IC spectrum are not so simple depending upon whether the majority of scatterings is in the Thomson or in the Klein-Nishina regime. In any case, our calculations indicate a good way to properly model the observed spectra. We also consider the case in which the probability of statistical acceleration is constant below a critical energy, thus producing a power law spectrum that turns into a log-parabola above this energy.

In the last part of the paper, we apply our model to the large flare from Mkn 501 observed in April 1997. This is a unique event in which the SR and IC components were observed simultaneously over energy bands that were broad enough to study the spectral curvature. We use the BeppoSAX data already analysed in Paper II together with those in the TeV band obtained by the CAT experiment (Djannati-Atai et al. 1999). Our approach of studying both the SR and IC spectral curvatures is useful for evaluating the relevance of the intergalactic absorption due to pair production from photon-photon interactions. In particular, we discuss the possibility that the observed TeV curvature is mainly intrinsic, as it implies rather low absorption and the possibility of detecting sources at larger distances than usually estimated.

2. Properties of the log-parabolic spectral distribution

The log-parabolic model is one of the simplest ways to represent curved spectra when these show mild and nearly symmetric curvature around the maximum instead of a sharp high-energy cut-off like that of an exponential. In the following, we summarise the main properties of log-parabolic spectra, while for details we refer to Papers I and II. This law has only one more parameter than a simple power law and can be written as:

$$F(E) = K(E/E_1)^{-(a\,+\,b\,\mathrm{Log}(E/E_1))}. \tag{1}$$

The energy dependent photon index is

$$\alpha(E) = a\ +\ 2\,b\,\mathrm{Log}(E/E_1). \tag{2}$$

With $\nu_\mathrm{p} = E_\mathrm{p}/h$ we also indicate the peak frequency of the SED where E_p is related to the spectral parameters of Eq. (1) as follows:

$$E_\mathrm{p} = E_1\ 10^{(2-a)/2b} \tag{3}$$

and

$$\nu_\mathrm{p}F(\nu_\mathrm{p}) = KE_1E_\mathrm{p}(E_\mathrm{p}/E_1)^{-a/2} = KE_1^2\ 10^{(2-a)^2/4b}. \tag{4}$$

It is useful to note that the above formulae must be used when working with photon spectra, as is usual in X and γ-ray astronomy. Energy spectra are obtained by multiplying Eq. (1) by E, and the corresponding spectral index is therefore increased by unity. In the following, we indicate the energy index with $a_\mathrm{e} = a - 1$ to avoid confusion. In this case the peak frequency becomes:

$$\nu_\mathrm{p} = \nu_1\ 10^{(1-a_\mathrm{e})/2b}. \tag{3$'$}$$

An advantage of the log-parabolic model compared to other curved spectral laws is that the curvature around the peak is characterised only by the parameter b, while in other models, like the continuous combination of two power laws, it is a function of more parameters. Note also that the estimate of b is independent of the particular spectral representation adopted for the data. The same property does not hold for the spectral-curvature parameter (SCP) defined by Sohn et al. (2003). Unlike b, this quantity depends upon the energy (frequency) interval chosen to estimate the spectral indices at high α_h and low α_l frequencies. The relation between b and SCP can be obtained by evaluating α in two energy ranges E_h (high) and E_l (low) from Eq. (2):

$$\mathrm{SCP} = \frac{\alpha_\mathrm{h} - \alpha_\mathrm{l}}{\alpha_\mathrm{h} + \alpha_\mathrm{l}} = \frac{b\,\mathrm{Log}(E_\mathrm{h}/E_\mathrm{l})}{a + b\,\mathrm{Log}(E_\mathrm{h}E_\mathrm{l}/E_\mathrm{l}^2)}. \tag{5}$$

For flat spectrum sources with a close to zero, SCP becomes practically independent of b.

One limit of the log-parabolic model, however, is that it can represent only distributions symmetrically decreasing with respect to the peak frequency. However, it is not difficult to modify Eq. (1) to take into account a possible asymmetry with respect to E_p. For instance, one can use two different values of b for energies lower and higher than E_p, where the two branches continuously match. An interesting possibility, which can be

simply explained in terms of the energy dependence of the particle acceleration probability (see next section), is that the low energy segment of the spectrum follows a single power law with photon index α_0 and that the log-parabolic bending becomes apparent only above a critical value E_c. This behaviour can be described by the following model that takes into account the continuity conditions on the flux and on $\alpha(E)$ at E_c:

$$\begin{aligned} F(E) &= K(E/E_1)^{-\alpha_0}, \qquad E \le E_c \\ F(E) &= K(E/E_c)^{b\ \mathrm{Log}(E_c/E_1)} \\ &\quad \times (E/E_1)^{-(\alpha_0 + b\ \mathrm{Log}(E/E_c))}, \qquad E > E_c. \end{aligned} \tag{6}$$

3. Statistical particle acceleration and log-parabolic spectra

In Paper I we showed that a log-parabolic distribution is not only a simple mathematical tool for spectral modelling, but that it also relates to the physics of the statistical acceleration process under some simple hypotheses. In the following, we extend the considerations of Paper I. The results, useful to derive some relations between the acceleration parameters, should not be considered as a complete theory of energy-dependent acceleration. To confirm the main findings of this approach, more detailed analytical and numerical calculations are necessary, but such a detailed theoretical approach is beyond the purpose of the present paper.

3.1. Energy distribution of accelerated particles

The energy spectrum of particles accelerated by some statistical mechanism, e.g. a shock wave or a strong perturbation moving down a jet, is given by a power law (Bell 1978; Blandford & Ostriker 1978; Michel 1981). In Paper I we showed that a log-parabolic energy spectrum is obtained when the condition that the acceleration probability p is independent of energy is released and that its value at the step i satisfies a power law relation as:

$$p_i = g/\gamma_i^q, \quad (i = 0, 1, 2, ...) \tag{7}$$

where g and q are positive constants. Such a situation can occur, for instance, when particles are confined by a magnetic field with a confinement efficiency that decreases for an increasing gyration radius. In Paper I (Sect. 6.1) we found that the integral energy distribution of accelerated particles is given by a log-parabolic law:

$$N(>\gamma) = N_0(\gamma/\gamma_0)^{-[s-1+r\,\mathrm{Log}(\gamma/\gamma_0)]}, \tag{8}$$

with

$$s = -\frac{\mathrm{Log}(g/\gamma_0^q)}{\mathrm{Log}\,\varepsilon} - \frac{q-2}{2}, \tag{9}$$

$$r = \frac{q}{2\,\mathrm{Log}\,\varepsilon}, \tag{10}$$

where γ_0 is the minimum Lorentz factor in Eq. (7). As already discussed in Paper I the differential energy distribution $N(\gamma)$ is not an exact log-parabolic law, but differs from it only by a logarithmic term and can be approximated well by a log-parabola with a very similar curvature over an energy range of several decades.

Shock wave acceleration is not the only statistical mechanism active in non-thermal sources. For instance, electron acceleration can occur in magnetohydrodynamical turbulence in which regions of magnetic field reconnection can develop in a very stochastic way. Recently, Nodes et al. (2004) presented the results of the numerical simulations of a relativistic particle acceleration in a three-dimensional turbulent electromagnetic field configuration, also taking their SR into account. These authors found energy spectral distributions that where significantly flatter than $s = 2$ and, in a few cases, characterised by a steepening spectral index at high energies. We verified that over sufficiently wide energy ranges, the spectra given by Nodes et al. (2004) are represented well by a log-parabolic law or by a combination of a power law and a parabola. The resulting curvature parameters are generally small, but probably the curvature depends on the distribution and size of the acceleration regions, so one can expect that, under different assumptions, it could be higher. Nodes et al. (2004) computed the emerging SR spectra, which show an appreciable curvature over a few decade frequency range.

Statistical acceleration is not the only way to obtain curved electron spectra. Energy distributions showing a rather mild curvature have also been obtained in blazar physics. To model the SED of MeV blazars, Sikora et al. (2002) assumed that electrons are accelerated via a two-step process with a broken power-law energy distribution as injection. When the cooling effects are taken into account, the resulting electron spectrum (see, for instance, Fig. 6 in their paper) can be described well by a log-parabola over a range that is wider than three decades, as we verified (in this case we found $r = 0.44$).

The assumption of Eq. (7) about the energy dependence of the acceleration probability can be modified to take other escape processes into account. For instance, one can assume that the acceleration probability is constant for low energies and that it begins to decrease above a critical Lorentz factor γ_a (see, for instance Eq. (23) in Paper I). An approximate expression for the energy distribution of accelerated particles under this condition for $\gamma \ll \gamma_a$ should follow a power law with spectral index $s_0 = -(\mathrm{Log}\ g)/(\mathrm{Log}\ \varepsilon)$, while for $\gamma \gg \gamma_a$ it will approximate a log-parabolic spectrum like Eq. (8):

$$\begin{aligned} N(\gamma) &= N_0\,(\gamma/\gamma_0)^{-s_0} \quad \gamma \le \gamma_0 \\ N(\gamma) &= N_0\,(\gamma/\gamma_0)^{-(s_0 + r\ \mathrm{Log}(\gamma/\gamma_0))} \quad \gamma > \gamma_0, \end{aligned} \tag{11}$$

where for the sake of simplicity we take $\gamma_0 = \gamma_a$. In addition to the power law and log-parabolic segments, we can also expect a sharp high-energy cutoff that appears when losses make the acceleration process highly inefficient.

4. Spectral properties of the emitted radiation

4.1. Synchrotron spectrum

It is important to know the relations between the spectral parameters a and b of the emitted radiation and those of the electron population, namely s and r. The spectral distribution of the SR by relativistic electrons having a log-parabolic energy

distribution cannot be computed analitically. For our purpose, however, the relations between the spectral parameters can be derived under the usual δ–approximation and the assumption that the electrons are isotropically distributed in a homogeneous randomly oriented magnetic field with an average intensity B

$$j_S(\nu) = \int P(\nu(\gamma))N(\gamma)\,\mathrm{d}\gamma \tag{12}$$

where j_S is the synchrotron emissivity, $N(\gamma)$ the electron density, and the power radiated by a single particle is

$$P(\nu) = \frac{4e^4}{9m^2c^3}\,\gamma^2B^2\,\delta(\nu-\nu_S), \tag{13}$$

and

$$\nu_S = 0.29\frac{3e}{4\pi mc}\,\gamma^2B \tag{14}$$

is the SR peak frequency for a single particle. We then obtain (see Paper I):

$$P_S(\nu) \propto N_0B^2(\nu/\nu_0)^{-(a+b\mathrm{Log}(\nu/\nu_0))} \tag{15}$$

with

$$\begin{aligned} a &= (s-1)/2 \\ b &= r/4. \end{aligned} \tag{16}$$

Note that the parameter a, as defined above, does not coincide with the one defined in Eq. (2), because the former is the energy index at the frequency ν_0, whereas the latter is the photon index at the energy E_1, not necessarily corresponding to ν_0. It is not difficult to verify that these two parameters differ for an additional constant, whose value depends on ν_0 and $\nu_1 = E_1/h$. In Paper I we noted that one can expect a and b to show a linear correlation, which was indeed found for Mkn 421. We stress that such correlation is not a general result that can be applied to any sample of sources. It also depends upon the values of q, g, and γ_0, which can be different from source to source, and the dispersions of their distribution functions can introduce a significant amount of scatter in the data that could destroy the correlation. Reasonably, one has to expect that the linear correlation between a and b can be found only when the physical conditions in the acceleration region are quite similar. The absence of correlation found by Perlman et al. (2005) in their sample, therefore, does not imply that curved spectra in blazars are not originated by energy-dependent statistical acceleration.

The relation between r and b given above (Eq. (16)) is not exact: one can expect that a precise calculation of the spectral curvature of the emitted radiation must give a b value smaller than in the δ approximation and that, for high values of r, b can be greater than unity (depending on the frequency interval used around the peak in which it is estimated) because of the exponential cutoff by the SR spectrum radiated by a single particle.

To compute the relations between the spectral parameters numerically and to study the spectral evolution of the emitting particles, as reported in the next subsection, we applied a time-dependent numerical code (Tramacere & Tosti 2003; see Tramacere 2002, for a detailed description of the code). This

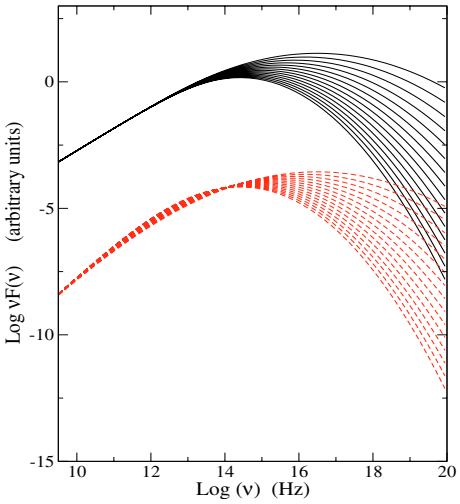

Fig. 1. Synchrotron spectra emitted by an electron population with log-parabolic (dashed lines) and power-law log-parabolic energy distributions (Eq. (11)) (solid lines), computed for r values in the interval 0.50–1.20. Spectra were shifted on the vertical scale to avoid confusion.

code uses a numerical integration routine that applies a modified Simpson rule ensuring good convergence in short computing times. In particular, this code includes an accurate evaluation of the synchrotron frequency distribution (hereafter SFD):

$$P(\nu) = \frac{\sqrt{3}e^3}{mc^2}B\frac{\nu}{\nu_c}\int_{\nu/\nu_c}^{\infty}K_{5/3}(x)\,\mathrm{d}x \tag{17}$$

where $K_{5/3}(x)$ is a modified Bessel function of the second type and ν_c the synchrotron critical frequency (Blumenthal & Gould 1970; Rybicki & Lightman 1979). Note that while the maximum of $P(\nu)$ is at $0.29\ \nu_c$, the peak in the corresponding SED $\nu P(\nu)$ is at the frequency $\nu_{pS} = 1.33\ \nu_c$.

We calculated the SR spectra and SEDs from Eq. (12) using a log-parabolic distribution without (LP) and with a low-energy power law branch (LPPL) (Eq. (11)) and the frequency distribution of Eq. (17). All the calculations in this and in the following subsections are performed in the co-moving frame, so relativistic beaming effects were not included.

Figure 1 shows some examples of the resulting SEDs. In these computations we assumed a uniform magnetic field $B = 0.14$ G, and the spectral parameters for the electrons were $\gamma_0 = 10^3$, $s = s_0 = 1.2$ (Eq. (11)), while r values were increased from 0.5 to 1.20 by steps of 0.05. The electron density and the size of the emission region were taken to be equal to the typical values used in blazar modelling. In these conditions the synchrotron self-absorption is important at frequencies lower than $\sim 10^{10}$ Hz. Note in Fig. 1 that at low frequencies both spectral sets tend to a power law: in the LP case the spectral index corresponds to the SFD asymptotic behaviour ($\nu^{1/3}$), while in the other case it has the energy spectral index $\alpha_{e0} = (s_0-1)/2$. At high frequencies the log parabolic behaviour is very evident with a peak frequency decreasing for higher values of r, as expected from Eq. (3) since b is also increasing with r.

We first verified that the peak frequency in the SED of the SR component ν_{pS} is proportional to the Lorentz factor γ_p

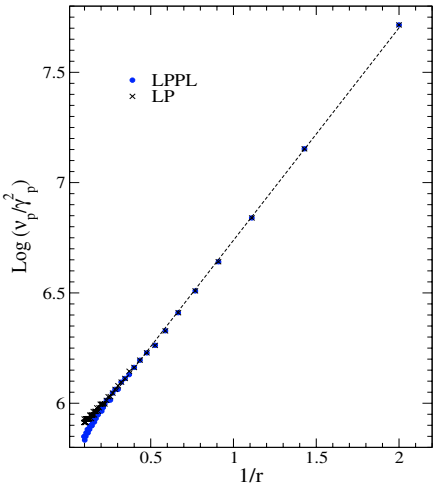

Fig. 2. The relation between the peak frequencies of the synchrotron SED and those of the energy spectrum of the emitting electrons computed using the SFD (Eq. (17)) for the LP and LPPL cases (see text). The abscissa is the inverse of the electron spectrum curvature to show the linear trend expected from Eq. (18). The dashed line is the best fit computed for $1/r > 0.33$. Note the small deviations of LPPL points from the best fit line at low values of $1/r$.

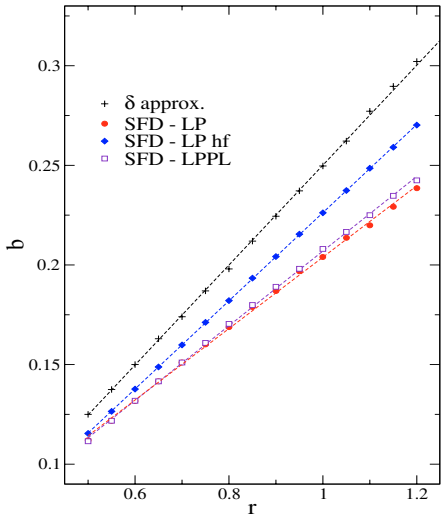

Fig. 3. The relation between the log-parabolic curvature parameters of the electron energy distribution r and those of the synchrotron radiation computed applying the δ approximation (crosses) and the SFD. The two LP point sets correspond to log-parabolic electron spectra with b evaluated by a best fit around the SED peak (filled circle) and on the high frequency branch (diamonds). LPPL points (open squares) correspond to a combined log-parabolic power law distribution. Dashed lines are linear best fits used for the calculation of the b/r ratio.

at which the electron distribution $\gamma^2\ N(\gamma)$ has its maximum. Applying the same formulae of Sect. 2, we have

$$\gamma_{\rm p} = \gamma_0 10^{(2-s_0)/2r}$$

from which we have:

$$\frac{\nu_{\rm pS}}{\gamma_{\rm p}^2} = \frac{\nu_0}{\gamma_0^2}\ 10^{1/r} \qquad (18)$$

where we assumed $\nu_0 = \nu_1$ for the sake of simplicity. In Fig. 2 we plotted the resulting $\nu_{\rm pS}/\gamma_{\rm p}^2$ vs. $1/r$ for both LP and LPPL cases: points of the two sets are coincident in the whole range of interest and only for $1/r < 0.3$ a small deviation from the linear trend of the LPPL model is evident. The slope of the best fit line (for $1/r > 0.3$) is equal to 0.97, very close to unity as in Eq. (18). Note also that the linear extrapolation to large values of r ($1/r \to 0$) gives for the $\nu_{\rm pS}/\gamma_{\rm p}^2$ ratio a value very close to 1.33 $\nu_{\rm c}$, consistent with the theory expectation.

We also used the spectra of Fig. 1 to study the relation between r and b under different conditions. The estimate of b is not simple because the radiation spectra do not have an exact log-parabolic shape. One can expect that this estimate is more accurate considering only the SED branches at frequencies higher than the peak: a quadratic best fit of the spectra of Fig. 1 confirms the linear relation between b and r, but the coefficient is equal to 0.22, slightly lower than the value found under the δ approximation (Eq. (16)). We also computed b considering a frequency interval centred at the peak frequency and spanning approximately two decades. The results are shown in Fig. 3. The relation between b and r was linear with very good accuracy, but the coefficient decreased to 0.18, as expected because of the smaller curvature of the low frequency branches. The last result does not change if the low energy electron spectrum follows a power law instead of a log-parabola (open squares in Fig. 3): the b/r ratio in this case was found equal to 0.19. We also verified our results by computing the spectra using the δ approximation and found $b/r = 0.2508$, in very good agreement with the theory. An approximate rule derived from this analysis indicates that it is convenient to take the value of the ratio equal to 0.2, within an accuracy of 10%. The resulting r estimate can then be used as the input value for a more refined modelling of the SED.

4.2. Spectral evolution under synchrotron cooling

We also studied the evolution of spectral curvature due only to synchrotron cooling. Of course, this study cannot be performed in general because the solution of the time-dependent continuity equation is a function of the assumed time evolution of the injection rate of emitting electrons and of several other parameters like the mean residence time of particles inside the emitting volume. We studied, therefore, the simplest case of a pure radiative SR cooling in a homogeneous and steady magnetic field without leakage and with a log-parabolic initial spectrum. The time evolution of SR and electron spectra are shown in the two panels of Fig. 4, where the decrease in both the peak frequency and intensity with time is very evident. Although radiation losses modify the spectral shape, it remains approximately log-parabolic, though with larger curvature parameters. These variations are shown in Fig. 5, where we plotted the r and b values, measured in energy/frequency intervals centered approximately at the distribution peaks, as a function of time, measured in units of the cooling time for the peak energy of the initial electron spectrum, taken as $\gamma = 10^5$ and corresponding to $\sim 5 \times 10^5$ s with a magnetic field $B = 0.1$ G. It is worth noting that the change in time of r and b is described well by

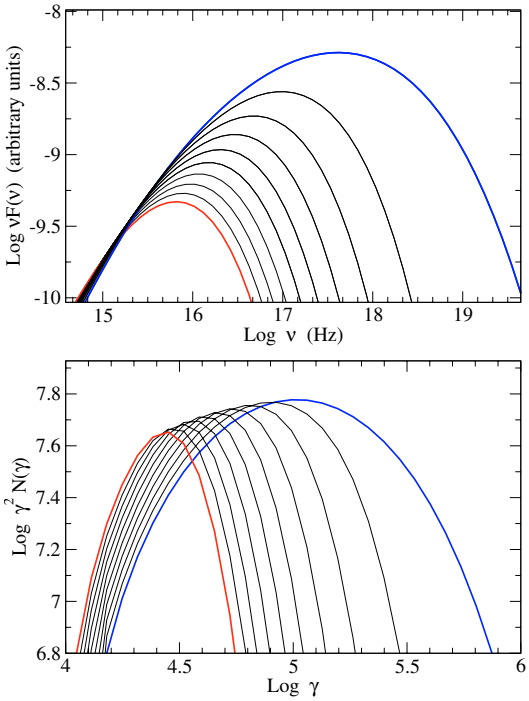

Fig. 4. Time evolution of the SR spectrum (*upper panel*) and of the corresponding spectrum of electrons, multiplied by the square of the Lorentz, under SR losses. The injection spectrum was a log-parabola with $s = 1.2$ and $r = 0.7$, corresponding to a peak energy of $\sim 10^5$. Spectra are plotted for equal time steps of ~0.4 cooling times. Note the decrease in the peak energy and the deviation from a log-parabola due to difference in cooling time with γ.

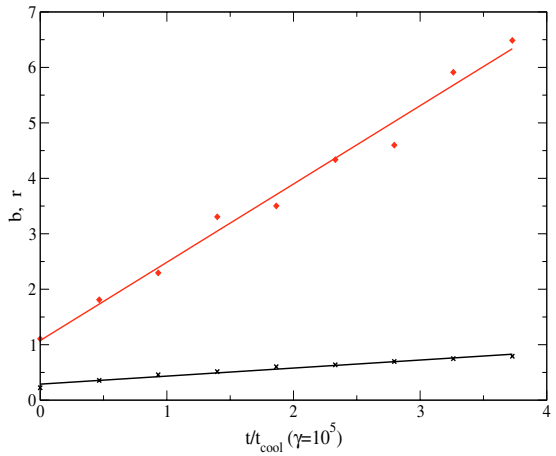

Fig. 5. Time evolution of the log-parabolic curvature parameters r of the electron spectrum (*upper line*) and b of the SR SED (*lower line*) computed by means of a best fit around the peak. Solid lines are linear best fits to the computed values.

linear relations. The observation of a decrease in $\nu_{\rm ps}$ associated with an increasing curvature during the dimming phase of an outburst is an indication of a radiative cooling evolution. Our calculations also show that the changes of SR peak frequency and b are correlated according to a power law as shown in the plot of Fig. 6.

We stress, however, that the estimate of b may not be simple when working with observational data because the position

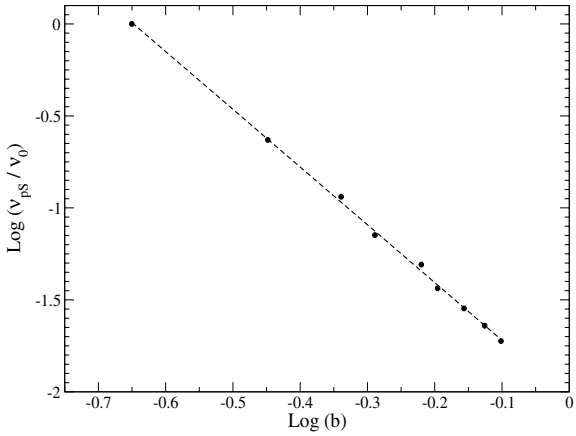

Fig. 6. The relation between the peak frequency and the curvature parameter b of the SR spectra plotted in the upper panel of Fig. 4. The dashed line is the best fit to the computed values.

of the peak may be far from the centre of the detector frequency range, and the uncertainty on the interstellar and intrinsic absorption may be non-negligible, particularly in the soft X-ray band.

4.3. Synchrotron Self-Compton spectrum

We computed the spectral distribution of the SSC emission from a relativistic electron population with a log-parabolic energy spectrum in the framework of a homogeneous one-zone model in which the seed photons are isotropic in the bulk frame of the electrons. Our goal is to estimate the relations between the main spectral parameters: the peak frequencies of the SR and IC components and their curvatures indicated in the following by b_S and b_C, respectively.

The IC emissivity is given by (Jones 1968; Blumenthal & Gould 1970; Band & Grindlay 1985)

$$j_{\rm C}(\nu') = (h\nu')\, c \int {\rm d}\nu\, n(\nu) \int {\rm d}\gamma\, ({\rm d}\sigma/{\rm d}\nu')\, N(\gamma) \qquad (19)$$

where $n(\nu)$ is the density of SR photons, ν' the frequency of scattered photons, and the differential Klein-Nishina cross section is:

$$\frac{{\rm d}\sigma}{{\rm d}\nu'} = \frac{3\sigma_{\rm T}}{16\gamma^4\nu}\left[2\eta\ln\eta + (1+2\eta)(1-\eta) + \frac{1}{2}(1-\eta)\frac{[4(h\nu/m_{\rm e}c^2)\gamma\eta]^2}{1+4(h\nu/m_{\rm e}c^2)\gamma\eta}\right] \qquad (20)$$

with

$$0 \le \eta = \frac{\nu'}{4\gamma^2\nu[1-(h\nu'/m_{\rm e}c^2)]} \le 1 \qquad (21)$$

and

$$1 \le \frac{\nu'}{\nu} \le \frac{4\gamma^2}{1+4\gamma(h\nu/m_{\rm e}c^2)}. \qquad (22)$$

Figure 7 shows two sets of resulting spectral distributions of both SR and IC components for values of r ranging from 0.5

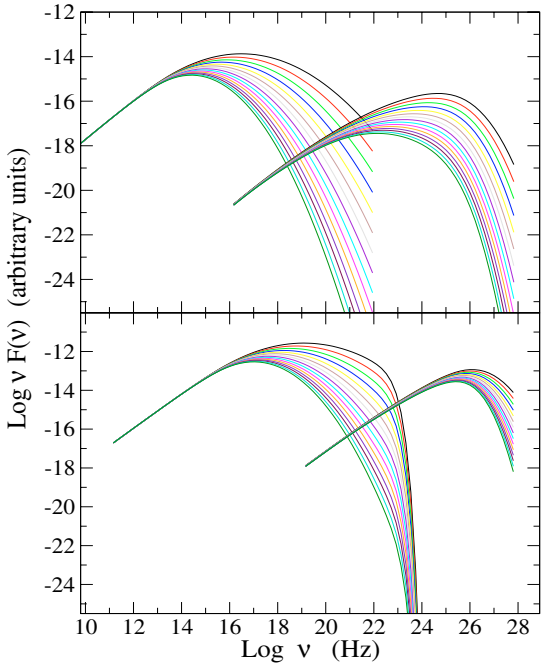

Fig. 7. The SR and SSC spectral energy distributions emitted by an electron population with power-law log-parabolic distributions (Eq. (11)), computed for r values in the interval 0.50–1.20. *Upper panel*: spectra for $\gamma_0 = 10^3$; *lower panel*: spectra for $\gamma_0 = 2 \times 10^4$.

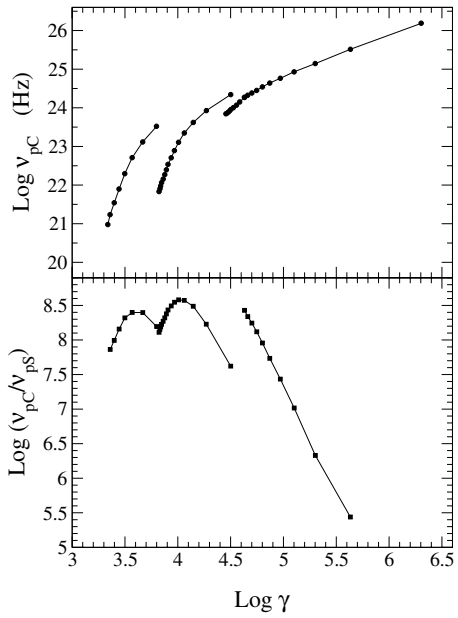

Fig. 8. Dependence of the peak frequencies upon the particle characteristic energies in the SED of a single zone SSC model. *Upper panel*: frequency of SSC peak vs. electron Lorentz factors of the peaks for r values in the interval 0.50–1.90, the three curves correspond to $\gamma_0 = 10^3$ (filled circles), 5×10^3 (open cicrcles), 10^4 (crosses). *Lower panel*: ratio between the peak frequencies of IC and SR components for the same values of the spectral parameters.

to 1.2 and γ_0 equal to 10^3 (upper panel) and 2×10^4 (lower panel). The upper cut-off of the energy electron spectrum was fixed at $\gamma_{ct} = 5 \times 10^7$. In the upper panel of Fig. 8, we plotted the peak frequency of the IC component ν_{pC} vs. γ_p for $\gamma_0 = 10^3$, 5×10^3, 10^4 and r ranging from 0.5 to 1.9. These curves are useful for understanding at which electron peak energy the IC emission is dominated by the Thomson or the Klein-Nishina regime. We stress that this does not imply that the largest contribution to the emission around ν_{pC} is due to electrons exactly at γ_p. We computed these energies and found that, for the highest value of γ_0, the difference is on the order of a few percent, while for the lowest γ_0 and $r = 1.7$ the greatest contribution to the IC peak is produced by electrons having $\gamma \simeq 6.3 \times 10^3$, while γ_p is at 1.4×10^4. It is of course impossible to derive a simple rule because of the number of parameters involved. Figure 8 (upper panel) shows that as γ_p increases, the corresponding ν_{pC} grows slower and slower indicating that the Klein-Nishina suppression becomes more efficient. A second way to show the relation between SR and IC components is given in the lower panel of Fig. 8, where we plotted the ratio ν_{pC}/ν_{pS} vs. γ_p: this ratio increases until the Thomson scattering is dominant and reaches the maximum at the transition to the Klein-Nishina regime.

The IC spectra show an evident curvature that is not univocally related to the r as in the SR case. Spectral curvature, in fact, depends on several parameters in a complex way. The spectral shape is generally different from a log-parabola, and it can be approximated by this function only in a limited frequency interval. Consequently, the estimate of the curvature parameter depends on the postion and amplitude of this interval. In particular, the curvature depends on the intrinsic electron spectral curvature, the energy of SR photons, and on the energy of the electrons that mostly contribute to the emission in the selected interval. These energies, in fact, determine if the scatterings happen in the Thomson limit or in the Klein-Nishina regime. We obtained spectra with a curvature less pronounced than SR only for $\gamma_0 = 10^3$ (i.e. for dominant Thomson scattering) and b evaluated in an interval around the peak. In all the other cases, higher b values of IC spectrum resulted. Figure 9 shows some examples: the curvature parameter b of the IC spectrum, computed in a single zone SSC model, was evaluated in three adjacent frequency intervals, each having an amplitude of about a decade starting from the peak frequency. When the main contribution to IC emission comes from Thomson scatterings, the curvature is closer to that of SR (solid line), and it approaches that of the electron spectrum (dashed-dotted line) when the fraction of interactions in the Klein-Nishina regime increases. The two panels correspond to γ_0 values differing by a factor of 20. In the upper panel, IC emission is dominated by Thomson scattering in the two first intervals, while in the lower panel the curvature approaches that of the electrons because the majority of interactions are in the Klein-Nishina regime. This property is really useful because a simultaneous measure of the curvature parameters of SR and IC emissions can help to discriminate between the two regimes of Compton scattering and to constrain the spectral parameters of emitting electrons.

5. The X-ray and TeV emission from Mkn 501

In Paper II we presented the results of analysing all BeppoSAX observations of the nearby HBL object Mkn 501 using

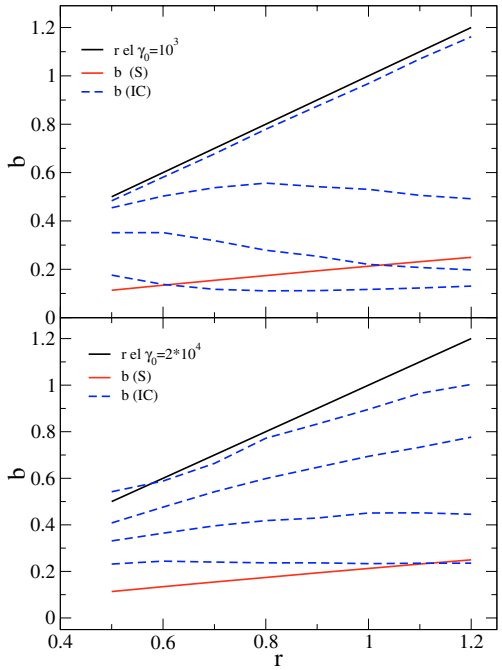

Fig. 9. The curvature parameter b of the IC spectrum for a single zone SSC model plotted against the electron spectral curvature r. Dashed-dotted lines are the curvature parameters for the electrons and solid lines for SR component. Dashed lines correspond to IC curvatures evaluated in three adjacent frequency intervals with an amplitude of about a decade selected starting from ν_{pC}: lowest lines correspond to the intervals closest to the peaks and the highest ones to those at the highest frequencies. The upper panel shows b values computed for $\gamma_0 = 10^3$ and lower panel those for $\gamma_0 = 2 \times 10^4$. Note that when the largest contribution to IC emission is from Thomson scatterings (*upper panel*), curvatures are closer to those of SR, while in the Klein-Nishina regime (*lower panel*) b values result very close to r.

log-parabolic spectral models. In the case of this source, we did not detect significant variations of the X-ray flux during the individual pointings, but large luminosity changes were found between the three observations of April 1997 (on the 7, 11, and 16) for which simultaneous TeV data, obtained with the CAT Cerenkov telescope, are available (Djannati-Atai et al. 1999). The TeV data showed a remarkable spectral curvature modelled by these authors by means of a log-parabolic law: best fit b values were higher than 0.4, while those measured in the X rays are in the range 0.12−0.17 (see Paper II). Krennich et al. (1999) observed Mkn 501 from February to June 1997 with the Whipple telescope and found a high curvature of the TeV spectra as well.

In Sect. 4 we discussed the relations between the parameters of log-parabolic spectra for a SSC emission and showed that SSC emission model can give high frequency spectra with a b value ranging from that of the SR component to that of the electron spectrum depending on whether the scattering occurs in the Thomson or in the Klein-Nishina regime. From the calculations of Sect. 3, we know that an SR b value of about 0.15 corresponds to $r \simeq 0.75$, and therefore a curvature of the IC component as that measured in the TeV range can be expected.

In Paper II we also presented a two component-model to describe the spectral evolution of the April 1997 X-ray outburst of Mkn 501. We assumed that the components had the same curvature ($b = 0.18$) and differ for the peak energy and their relative intensity. In this way we explained the nearly constant flux observed at lower energies than ∼1 keV, while that around 100 keV changed by more than one order of magnitude, and the slight decrease of b in the higher states was interpreted as the effect of the sum of two log-parabolic distributions peaked at different energies.

An important effect to be considered when computing the spectral curvature in the TeV range is the absorption of the most energetic photons due to pair production against the infrared extragalactic background light (EBL). Dwek & Krennich (2005) have recently studied twelve EBL models and computed the corresponding intrinsic spectra of Mkn 501. These authors found that the majority of EBL models give intrinsic emitted spectra showing an unphysical rise at high TeV energies and that only the lowest intensity EBL models are acceptable.

We applied our radiation code to searching for the geometrical and physical parameters of the emitting region that can reproduce the observed intensities and spectral shapes, also taking EBL absorption into account. To compare the model with the data, we need to introduce a relativistic beaming factor δ, which does not affect the spectral shape, but which changes observed frequencies and fluxes by $\delta/(1+z)$ and $[\delta/(1+z)]^3$, respectively, where $z = 0.034$ is the source redshift. In the following we assume $\delta = 15$, in agreement with other models for Mkn 501 (see e.g. Kataoka et al. 1999).

We first considered a single-zone SSC model and tried to reproduce the two extreme states of the large outburst of April 1997, i.e. the low state on April 7 and the high state on April 16.

The spectrum of the emitting electrons was chosen with a curvature parameter $r = b/0.2 \simeq 0.75$ following the relation found in Sect. 4.1, and the parameter s was fixed to 1.2. Note that this value of r is consistent with the general behaviour presented in Fig. 9. The TeV curvature measured around the peak was about 0.4 for the low state and 0.45 for the high state (Djannati-Atai et al. 1999) and, for γ_0 on the order of 10^4 and even higher, we expect a value of r in the range 0.5−0.8. The values of the other parameters, given in Table 1, were chosen to achieve a satisfactory agreement between the data and the model. It is interesting to note the behaviour of the two correlated parameters ν_{pS} (the peak frequency in the synchrotron SED) and γ_p (the value of γ of the electrons that contribute mostly to synchrotron peak emission). In fact the ν_{pS} grows during the flare by a factor of 11 compared to the initial value while, according to Eq. (14), γ_p changes as the square root of ν_{pS} growing rate. Spectral distributions of Fig. 10 show that the SR follows the X-ray data accurately in both the spectral shape and peak evolution. The TeV spectra in the two states were computed using the SSC code described in Sect. 4.2: in the upper panel of Fig. 10 we considered the EBL absorption for the LLL model by Dwek & Krennich (2005), while in the lower panel this absorption was neglected. In both cases TeV data were well fitted in both the peak position and spectral curvature. This suggests that this curvature could be partly intrinsic rather than produced entirely by EBL absorption.

Table 1. Model parameters for the 1997 April flare of Mkn 501.

Date	s	r	N cm^{-3}	γ_0 10^4	γ_p 10^5	V cm^3	E_e 10^{44} erg	$\nu L_\nu(SR)$ 10^{39}erg/s	$\nu L_\nu(IC)$ 10^{39}erg/s	B G	δ
SSC - 1 zone											
Apr. 07	1.12	0.81	4.25	4.80	1.67	1.57×10^{47}	91.0	8.70	4.47	0.10	15
Apr. 16	1.18	0.70	30.0	8.70	3.36	1.72×10^{46}	90.6	34.60	21.4	0.14	15
SSC - 2 zones											
Apr. 07 (Z1)	1.14	0.81	4.6	4.0	1.35	1.2×10^{47}	57.9	8.71	3.42	0.14	15
Apr. 11 (Z2)	1.2	1.00	1050	14	3.52	9.2×10^{40}	0.156	6.92	1.44	1.5	15
Apr. 16 (Z2)	1.2	1.33	250	20	3.95	9.2×10^{43}	6.12	29.5	14.1	0.2	15

V is the volume of the emitting region; E_e is the total energy of radiating electrons; $\nu L_\nu(SR, IC)$ are the SED peak values of SR and IC components, respectively.

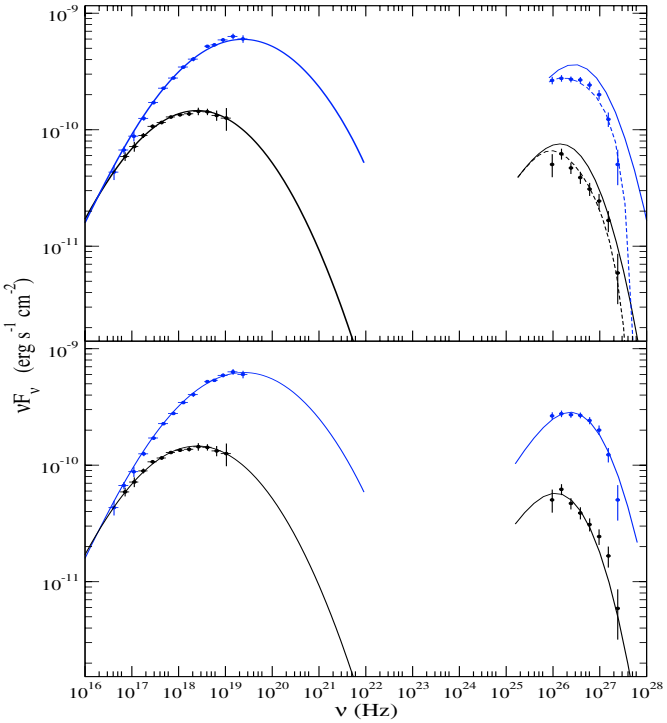

Fig. 10. Two spectral energy distributions of Mkn 501 during the low and high states observed on 7 and 16 April 1997, respectively. X-ray points are from Paper II, TeV points are simultaneous CAT data (Djannati-Atai et al. 1999) and soolid lines are the spectra computed in a 1-zone SSC model for the SR and IC components. In the upper panel IC, spectra have been absorbed (dashed lines) by interaction with infrared EBL photons according to the LLL model by Dwek & Krennich (2005). In the lower panel EBL absorption was neglected.

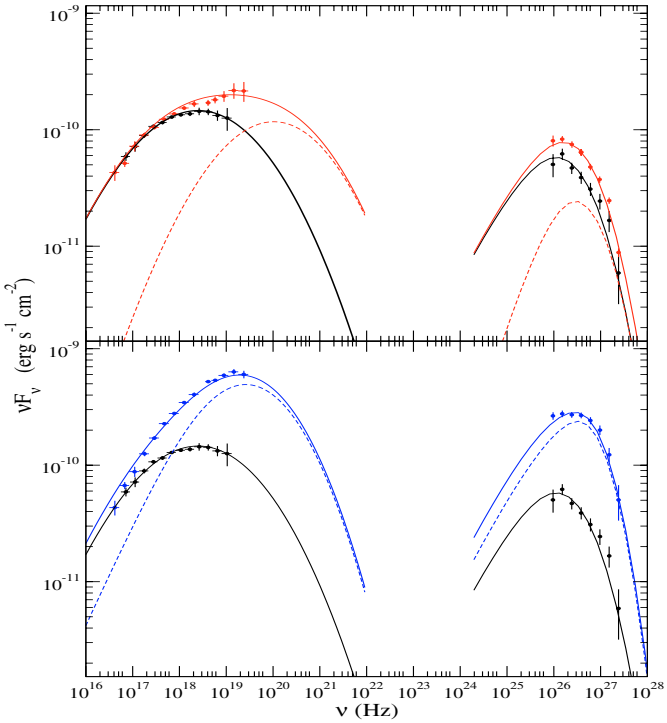

Fig. 11. Two spectral energy distributions of Mkn 501 during the high states observed on 7, 11 April 1997 (*upper panel*) and 7, 16 April 1997 (*lower panel*). X-ray points are from Paper II, and TeV points are simultaneous CAT data (Djannati-Atai et al. 1999). Thin solid lines are the spectra computed in a 2-zone SSC model for the SR and IC components, dashed lines are the spectra of the high-energy flaring component, and the thick solid line is that of a slowly evolving component.

The LLL model could then be considered an upper limit to the extragalactic background.

As proposed in Paper II we considered a two-zone SSC model. A first zone (Z1) is responsible for the "slowly" variable emission, whereas the second zone (Z2) is the source of the high-energy flare: the observed fluxes are then the sum of these two contributions. We used the April 7 emission as representative of the "slowly" variable state (Z1) and added the flaring component (Z2) to match the April 11 and 16 high states. In this way the stability of the flux at energies $\leq$1 keV is easily explained by the fact that the emission from Z2 is negligible when compared with that of Z1. The results of these calculations are represented in the SEDs of Fig. 11. We met some difficulty in obtaining a solution capable of modelling the observed spectral curvature mostly in the highest state. In fact, to deplete the SR from Z2 below ~1 keV, we need an electron population with a very low emissivity in this band. This can be obtained only by introducing a low energy cut-off, with the consequence of a high curvature of the low energy portion of IC spectra at TeV energies. The values of parameters for this 2-zone SSC model are also given in Table 1.

These results can be used to obtain some information on the acceleration process. According to Eq. (10) we can derive the energy gain as a function of r:

$$\varepsilon = 10^{q/2r} \tag{23}$$

which, given that $r \simeq 1.0$, gives $\varepsilon \simeq 3.2^q$. This implies that, unless q is very small, the energy gain is about a factor 3. Consequently, the number of steps to increase the energy up to $\gamma \simeq 10^5$ is around 10. The acceleration must therefore be efficient and should probably occur for rather short times.

It is interesting to compare our SEDs of the 1997 flare of Mkn 501 with those calculated by other authors who adopted different physical models. Generally, there is no explicit evaluation of a spectral curvature parameter for both SR and IC components and consequently the electron energy distributions are assumed to be power laws with exponential cut-off (Konopelko et al. 2003; Krawczynski 2002) or a broken power law (Katarzynski 2001).

To reproduce the spectral curvature in IC spectra, these authors need to introduce a heavy contribution from EBL interaction with TeV photons. We stress that in our analysis the SR curvature is intrinsic, and we do not need break or cut-off to reproduce it. More interestingly, the IC curvature is also intrinsic and can be reproduced both using and neglecting the TeV photon absorption by EBL photons. In particular in the, in case of large flares where the peaks of SR and IC components increase their energy, models with break or cut-off do not predict intrinsically curved IC spectra, and so the spectral shape observed at TeV and the IC peak frequency are mainly modulated by what EBL model is chosen. Note also that EBL attenuation could consistently modulate the position of the IC peak because its optical depth varies with the energy and redshift. Observations of SR and IC components in objects with different redshifts and the study of the variations of their peak frequencies would be very useful for more accurate modelling of the EBL spectrum.

It is interesting to compare the values of the main model parameters. As a further point Konopelko et al. (2003) and Krawczynski et al. (2002) used δ values of 50 and 45, respectively, while Katarzynski et al. (2001) used 14, very close to our choice.

6. Summary and conclusion

Over the past decade, broad-band observations of blazars have clearly shown that their non-thermal SEDs are characterised by mildly curved shapes that can be approximated by simple power laws only in frequency intervals that generally not wider than a single decade. Starting from the first paper by Landau et al. (1986), we verified that a log-parabolic law is instead able to represent blazars' SEDs over several frequency decades. An advantage of this law is that it has only three free parameters. Furthermore, we have shown that for statistical acceleration mechanisms in which the acceleration probability is a decreasing function of the particle energy, as in Eq. (7), the resulting spectrum follows a log-parabolic law. Spectral properties of the SR can be derived easily only by using the δ-function approximation.

To find the exact relations between the spectral parameters of the energy distribution of the relativistic electrons and of their SR, we used a precise numerical code specifically developed for blazar applications. The main results can be summarised as follows:

- the SR spectrum is log-parabolic with a curvature parameter approximately equal to the electron curvature parameter multiplied by 0.2;
- spectral evolution due to SR cooling maintains a log-parabolic distribution whose curvature parameter increases linearly with time;
- the IC SED around the peak can be approximately described by a log-parabola having a curvature parameter that ranges from values lower than the SR spectrum up to that of the electron distribution, depending upon whether the photon scattering is in the Thomson or Klein-Nishina regime. The difference between the SR and IC curvatures can be used to discriminate between the two regimes.

We applied our code to the calculation of the SR and IC spectra of Mkn 501 when it was simultaneously observed by *BeppoSAX* (Paper II) and CAT (Djannati-Atai et al. 1999) during the large outburst of April 1997. We estimated the spectral parameters of the emitting electrons from X-ray data and then computed the IC spectrum in the TeV band, taking the absorption from pair production against EBL into account. Our results showed that the curvature at high energy is mostly intrinsic and larger than in the X-ray range, which shows that the IC scattering is taking place in the Klein-Nishina regime. This finding suggests that intergalactic absorption of TeV photons may be small, as shown by Dwek & Krennich (2005): their LLL spectrum could be a satisfactory description of EBL, but we cannot exclude that it has an even lower intensity. This interpretation agrees with a previous work by Krawczynski et al. (2000), where the low intensity DEBRA model (Malkan & Stecker 1998) was favored over another model of higher intensity. It is also supported by a recent paper by Aharonian et al. (2005a), who used HESS data to find that in the time-averaged observations of Mkn 421, the cutoff energy of the IC spectrum is at ~3.1 TeV, lower than that found in Mkn 501 (about 6.2 TeV). Considering the nearly equal redshifts of the these two blazars, they conclude that the cutoff is not due to EBL attenuation but is intrinsic to the sources, in agreement with our conclusion about the IC curvature. We conclude (i) that the extragalactic space is probably more transparent to TeV photons than previously assumed and (ii) that a larger number of blazars at higher redshifts than previously thought could be detected in this range.

The same conclusion has been reached very recently by Aharonian et al. (2005b), who report the detection of the blazar 1ES 1101−232 at $z = 0.186$ (by HESS in the TeV band). An important consequence of the intrinsic curvature of TeV spectra is that it can be variable in time and possibly related to the X-ray curvature. As a final remark, we stress the relevance of the simultaneous broad-band observations that are necessary to obtain a reliable estimate of curvature parameters for both components.

Acknowledgements. We acknowledge the helpful comments and suggestions of the referee, A. Djannati-Atai. This work was financially supported for the ASDC by the Italian Space Agency (ASI) and for the Physics Dept. by Università di Roma La Sapienza.

References

Aharonian, F., Akhperjanian, A. G., Aye, K.-M., et al. 2005, A&A, 437, 95
Aharonian, F., Akhperjanian, A. G., et al. 2005, Nature, submitted [arXiv:astro-ph/0508073]
Band, D., Matteson, J., Ford, L., et al. 1993, ApJ, 413, 281
Bell, A. R. 1978, MNRAS, 182, 147
Blanford, R. D., & Ostriker, J. P. 1978, ApJ, 221, L29
Blumenthal, G. R., & Gould, R. J. 1970, Rev. Mod. Phys., 42, 237
Djannati-Atai, A., Piron, F., Barrau, A., et al. 1999, A&A, 350, 17
Dwek, E., & Krennich, F. 2005, ApJ, 618, 657
Kardashev, N. 1962, Soviet Astron., 6, 317
Kataoka, J., Mattox, J. R., Quinn, J., et al. 1999, ApJ, 514, 138
Katarzyñski, K., Sol, H., & Kus, A. 2001, A&A, 367, 809
Konopelko, A., Mastichiadis, A., Kirk, J., et al. 2003, ApJ, 597, 851
Krawczynski, H., Coppi, P. S., Maccarone, T., & Aharonian, F. A. 2000, A&A, 353, 97
Krawczynski, H., Coppi, P. S., & Aharonian, F. 2002, MNRAS, 336, 721
Krennich, F., Biller, S. D., Bond, I. H., et al. 1999, ApJ, 511, 149
Landau, R., Golisch, B., Jones, T. J., et al. 1986, ApJ, 308, 78
Malkan, M. A., & Stecker, F. W. 1998, ApJ, 496, 13
Marscher, A. P., & Gear, W. K. 1985, ApJ, 298, 114
Massaro, E., Perri, M., Giommi, P., & Nesci, R. 2004a, A&A, 413, 489 (Paper I)
Massaro, E., Perri, M., Giommi, P., et al. 2004b, A&A, 422, 103 (Paper II)
Michel, F. C. 1981, ApJ, 247, 664
Padovani, P., & Giommi, P. 1995, ApJ, 111, 222
Nodes, C., Birk, G. T., Gritschneder, M., & Lesch, H. 2004, A&A, 423, 13
Perri, M., Massaro, E., Giommi, P., et al. 2003, A&A, 407, 453
Perlman, E. S., Madejski, G., et al. 2005, ApJ (in press) [arXiv:astro-ph/0502298]
Piranomonte, S., Giommi, P., Verrecchia, F., & Perri, M. 2002, in Blazar Astrophysics with BeppoSAX and other Observatories, ed. P. Giommi, E. Massaro, & G. Palumbo (ASI Special Publ.), 51
Sambruna, R., Maraschi, L., & Urry, M. C. 1996, ApJ, 463, 444
Sikora, M., Begelman, M. C., & Rees, M. J. 1994, ApJ, 421, 123
Sikora, M., Blazejowski, M., Moderski, R., et al. 2002, ApJ, 577, 78
Sohn, B. W., Klein, U., & Mack, K.-H. 2003, A&A, 404, 133
Tavecchio, F., Maraschi, L., Pian, E., et al. 2001, ApJ, 554, 725
Tramacere, A. 2002, Laurea thesis, Univ. of Perugia
Tramacere, A., & Tosti, G. 2003, New AR, 47, 697